Investigation on the influence of image quality in X-ray CT metrology

Müller, Pavel; Hiller, Jochen; Cantatore, Angela; Bartscher, Markus; De Chiffre, Leonardo

Publication date:
2012

Investigation on the influence of image quality in X-ray CT metrology

Pavel Müller[1], Jochen Hiller[1], Angela Cantatore[1], Markus Bartscher[2], Leonardo De Chiffre[1]

[1]Technical University of Denmark, Department of Mechanical Engineering,
Produktionstorvet, 2800 Kgs. Lyngby, Denmark,
e-mail: pavm@mek.dtu.dk, jochi@mek.dtu.dk, acan@mek.dtu.dk, ldch@mek.dtu.dk

[2]Physikalisch-Technische Bundesanstalt (PTB) Braunschweig und Berlin,
Bundesallee 100, 38116 Braunschweig, Germany, e-mail: markus.bartscher@ptb.de

Abstract
This paper presents a method for evaluating measuring errors in a CT system using information from quality of reconstruction images. In particular, spatial resolution and pixel noise are considered in this work. Both factors can be theoretically described using formulas, and can be expressed as a combination of scanning setting parameters. A 3^2 full factorial design of experiment (DOE) was carried out to determine the influence of the two factors on dimensional measurements. For quantification of the influence, an evaluation parameter sphere distance error was selected. Results show that the spatial resolution is a dominant factor. Analysis of the reconstruction images is carried out, showing image artifacts occurring on the spheres visible under large opening angle, which are usually more significant for CT scans at high magnification. Theoretical formulation of pixel noise was validated through the experimentation.

Keywords: Computed tomography, image quality, pixel noise, spatial resolution, dimensional CT measurement.

1 Introduction

Computed Tomography (CT) is becoming more and more accepted measuring technique [1]. Even though, measurement uncertainty in CT is in many cases unknown [2], CT has many advantages which make this imaging technique a very interesting tool. In CT, large number of influence factors is present in the whole process chain of CT measurement. Sometimes, identification and correction of these factors is a challenge. There are influence quantities related to software/data processing, hardware, measurement object, environment and operator. Influence factors and their effect on dimensional measurements have been widely studied by a number of authors [3-7].

One way to analyze the influence of several factors and their interaction at the same time is the application of design of experiment (DOE). This is a systematic approach to experimentation, when all the factors, defined at different levels, and their interactions, are considered simultaneously. In [3], for example, a fractional factorial DOE was carried out to investigate the effect of CT system parameters, which influence the imaging process and can be varied by the system operator. Tube voltage, tube current, pre-filter, exposure time and sensitivity of the detector were considered, each factor was investigated at two levels. The influence of each factor was assessed by calculation of the measurement uncertainty. In [4], a full factorial DOE was performed to investigate the influence of operator-related factors to dimensional CT. In particular, magnification, orientation, number of views and threshold method were considered to evaluate their influence on measurements of inner and outer diameter of parts of different material. Here, the factors were defined at two levels each.

This paper presents an investigation of the influence of several operator-related parameters on dimensional CT measurements. The focus is on parameters influencing the image quality. In particular, spatial resolution and pixel noise are considered.

2 Current approach

This paper introduces an alternative approach of experimental design in CT. The approach is based on defining factors through combination of scanning parameters (X-ray source current, integration time, image averaging, scanning geometry, etc.) and derived quantities in connection with the physical-technical characteristics of the X-ray tube (focus spot) and the detector system (resolution) as the two main system components. The two selected factors, *spatial resolution* and *pixel noise*, are well-known key characteristics describing the quality of CT images [8].

Spatial resolution in a volumetric CT image, U_{TOT}, is mainly influenced by the focus size, focus drift during scanning, contrast transmission of the detector system, reconstruction algorithm, and scanning geometry [8]. For simplification reasons, the focus size, the detector system, and the scanner geometry were taken into account only. The estimated spatial resolution, U_{TOT}, is then defined as [8]:

$$U_{\mathrm{TOT}} = \sqrt{U_{\mathrm{F}}^2 + U_{\mathrm{D}}^2} \qquad \text{(eq. 1)}$$

where U_{F} is geometrical unsharpness associated with focus size and U_{D} is geometrical unsharpness associated with the contrast transmission of the detector. Both can be described as follows [9, 10]:

$$U_{\mathrm{F}} = \frac{m-1}{m} \cdot W_{\mathrm{F}} \qquad \text{(eq. 2)}$$

$$U_{\mathrm{D}} = \frac{W_{\mathrm{D}}}{m} \qquad \text{(eq. 3)}$$

where m is geometrical magnification, defined as m = SDD/SRD with SDD as source-to-detector distance and SRD as source-to-rotation center distance [11]. W_{F} is size of the focus spot which is linked to the X-ray tube power [10, 12] and W_{D} is detector image unsharpness which is assumed to be double the pixel size [13]. Only two geometrical unsharpness parameters U_{F} and U_{D} were considered, also because they are the most dominant geometrical unsharpness sources.

The symbol of spatial resolution U_{TOT} should not be confused with measurement uncertainty which has typically the same symbol U.

Pixel noise, σ_{pn}, is expressed in the form of standard deviation evaluated in 2D slices of reconstructed images as follows [9, 14]:

$$\sigma_{\mathrm{pn}} = \frac{k \cdot \pi}{s \cdot \sqrt{V}} \cdot \frac{1}{\sqrt{I \cdot t \cdot i}} \qquad \text{(eq. 4)}$$

where
- k constant depending on a back-projection filter type, in our case k = 0.23 was chosen
- s pixel size in a 2D slice in mm^2
- V number of views (projections)
- I X-ray source current in mA
- t integration time of the detector in s
- i image averaging number

The pixel noise should not be confused with the noise in the projection images.
With the increase of X-ray source current and integration time, more photons are detected by the detector system. An increased number of photons and image averaging improve the detector image statistics, which follows a Poisson distribution, leading to an improved signal-to-noise ratio (SNR).
Based on the formulas described above (eq. 1 and eq. 4), a 3^2 full factorial DOE was assessed and is shown in Table 1. The two factors, spatial resolution and pixel noise, are defined theoretically by the assessment of scanning parameters at three levels, approx. equally distributed. The DOE was created in statistical software Minitab Release 14.1. This software is used to create a design to examine the relationship between factors. The design is fully randomized which helps to ensure that the model meets certain statistical assumptions. Column Run Order in the table indicates the order in which the data are collected.

Run Order	Voltage	Current	Magnif.	Voxel size	Full cone angle	Int. time	Image avg.	No. of views	Spatial res.	Pixel noise
	U in kV	I in mA	m	s in µm	α in °	t in s	i	V	U_{TOT} in mm	σ_{pn} in $mm^{-2}\cdot(mA\cdot s)^{-1/2}$
1	70	0.112	3.52	57	8.2	1.415	2	1200	0.114	0.65
2	70	0.112	7.04	28	16.2	2.829	4	1200	0.057	0.65
3	81	0.096	2.35	85	5.4	0.708	1	1200	0.170	0.94
4	78	0.100	3.52	57	8.2	0.708	1	1200	0.114	1.38
5	87	0.090	2.35	85	5.4	0.354	1	1200	0.170	1.37
6	78	0.101	7.04	28	16.2	2.829	1	1200	0.057	1.37
7	78	0.100	2.35	85	5.4	1.415	1	1200	0.170	0.65
8	72	0.109	7.04	28	16.2	1.415	4	1200	0.057	0.93
9	72	0.108	3.52	57	8.2	0.708	2	1200	0.114	0.94

Table 1: Experimental plan with calculated factors U_{TOT} and σ_{pn} from eq. 1 and eq. 4.

The individual positions of the object in the CT volume, i.e. positions of the object with respect to the X-ray source in the direction of the magnification axis, are shown in Figure 1. Explanation of the full cone angle α from Table 1 is also shown in the figure.

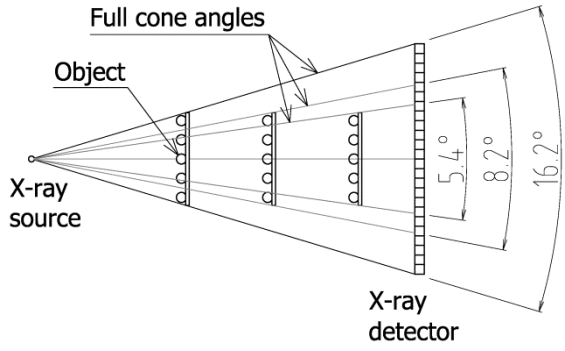

Figure 1: Three positions of the object (CT ball plate) (side view) in the CT volume according to the DOE plan presented in Table 1. The full cone angle at individual positions is specified.

In order to minimize the influence of the focus spot size, this was nominally kept constant by using constant power. The focal spot size was assumed to be approx. 1 µm per Watt tube power [12]. Since all the nine experimental runs yield different contrast, the corresponding X-ray tube power (X-ray tube current and acceleration voltage) were adjusted so, that the focus spot size was approx. 7 µm.

3 Experimental setup

A newly developed reference standard for metrological performance testing of CT systems – a CT ball plate [15] (Figure 2 left) was used in this study. This object features ruby spheres of diam. 5 mm in a regular 5 x 5 array with a nominal pitch between sphere centers of 10 mm. The spheres are glued on a 2 mm thick carbon fibre plate.

This reference standard is calibrated using a tactile coordinate measuring machine (CMM). The standard was measured at two positions, D0 and D180. In both positions all spheres were measured twice, once in a counter-clockwise and once in a clockwise spiral sequence. This procedure was repeated three times. The standard was also measured in different days to check the stability. The calibration involves measurements of center positions of the spheres, the sphere diameters and form errors. The expanded calibration uncertainty for measurements of distance between sphere centers, evaluated at 95% confidence level, was estimated to be 1.7 µm. The standard enables to evaluate 300 sphere-to-sphere distances in total.

The experiment was carried out using a Nikon Metrology XT H 225 ST CT scanner. FDK based reconstruction was done using software CT Pro V2.2 SP2 provided by Nikon Metrology, too. The CT ball plate was positioned vertically, and was not repositioned during individual runs of the experiment. The position of the object in Z direction (Z axis points from X-ray tube to the detector, see Figure 2 right) of the CT scanner's coordinate system was in accordance with Table 1.

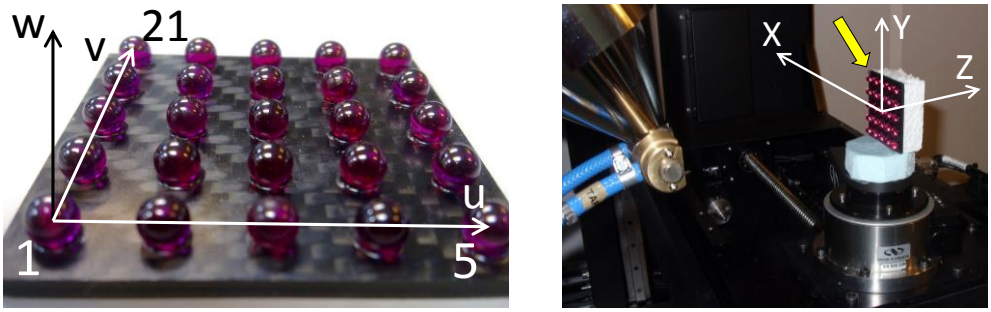

Figure 2: CT ball plate used for quantification of measurement errors in the CT volume, designation of the spheres and workpiece coordinate system (left) and measurement setup in the XT H 225 ST CT scanner (right). The CT ball plate was scanned in vertical position. The coordinate system of the CT scanner and the position of a thin metal plate (yellow arrow), indicating origin of the CT ball plate, are also shown.

4 Data evaluation

For determination of the surface, inspection software VG Studio Max 2.1 was used. Figure 3 presents a gray value distribution of the reconstructed volume. The three peaks correspond to air, carbon fibre and ruby. Since the automatic method for surface determination did not segment the air and ruby spheres, but air and carbon fibre (Figure 3 left), the segmentation was done manually by specifying the ruby spheres on the peak with material. Finally, advanced surface method was applied (Figure 3 right). Here, the vertical red line represents a starting value for threshold in adaptive surface determination.

As evaluation parameter, sphere distance error *SD*, was selected according to VDI/VDE 2630 – Part 1.3 [16]. *SD* is a robust parameter independent of errors due to a threshold determination, and it is a parameter used for correction of scaling errors. Other performance characteristics from this standard, i.e. probing error size *PS*, probing error form *PF* and length measurement error *E*, were not considered in this work, also due to size limitations of the paper. *SD* was evaluated at the upper hemi-spherical surface only, leaving out the part of spheres glued to the plate, which could lead to imperfections in measurements, possibly caused by noise. Approximately 1000 points were fit to define geometrical primitives ("half" spheres in our case).

The CT scans were corrected for scale errors by applying linear regression. A linear regression coefficient a is obtained by fitting a linear line through the whole data set of 300 single point deviations with its intersection in point [0,0]. A correction factor CF is calculated as $CF = 1/(a+1)$. This method was already introduced in [17]. The resulting corrected voxel size s_{COR} is given by multiplying the correction factor CF and the original voxel size s_0 as $s_{COR} = CF \cdot s_0$.

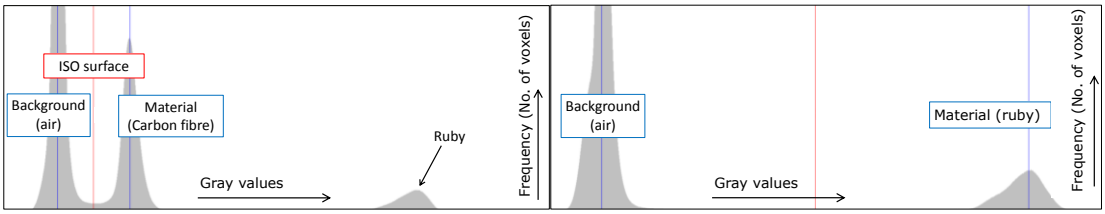

Figure 3: Histogram of gray values of the reconstructed volume and determination of ISO surface. By applying automatic threshold method, the surface is determined between the air (background) and carbon fibre (material) (left). A manual determination of the ruby material was carried out (right). Finally, the surface was determined using advanced threshold method. The red line represents a starting value for threshold in adaptive surface determination.

5 Results and discussion

Results of sphere distance errors (Figure 4) show that the errors in the present study are bigger at high geometrical magnification (= high resolution), approx. ±30 µm, and smaller at low magnification (= low resolution), approx. ±10 µm. This can be due to three reasons: Feldkamp effect [17], focus spot drift or rotary axis drift in X and Y directions [18] (for orientation see Figure 2 right). It is known that Feldkamp effect is most pronounced when an object is scanned at large opening angles. Table 1, among others, show that a cone angle at high magnification (α=16.2°) is approx. three times bigger than at low magnification (α=5.4°). Image artifacts, most likely caused by the Feldkamp effect, were observed on reconstruction images for CT scans at high resolution (see Figure 5). The potential impact of the focus drift is also most pronounced at high magnifications. At high magnifications, the difference between the focus drift and the drift of axis of the rotary table is small. Therefore, it is difficult to separate the three effects – Feldkamp, focus drift and rotary axis drift. Due to experience of the authors in general and with the CT system under study it is assumed for the series of measurements performed here that the Feldkamp effect is the most dominant of the three error types.

Figure 5 shows an example of a reconstructed image corresponding to Run 2 of the experiment, i.e. CT scan at high spatial resolution. Here, image artifacts at the upper and lower borders of the image can be recognized. The occurrence of the Feldkamp effect is more clear here. Image in this figure was taken in the XY plane of the CT scanner's coordinate system, and was slightly modified in *Fiji* software (free software for image analysis) to enhance the contrast and to better visualize the image artifacts.

Plot in Figure 6 shows results of one-factor effects, so called main effects, calculated in Minitab DOE software. In particular, the figure shows the influence of spatial resolution and pixel noise on data

scatter of *SD* parameter, expressed as 2*standard deviation of this parameter. Individual points in the graph represent a mean of all runs using individual level of either of the factors, i.e. in case of our DOE each data point corresponds to a mean value of three runs. One can observe, that the influence of spatial resolution on data scatter is clearly significant (steep nearly linear trend), compared to pixel noise, where this factor seems not to be significant (horizontal linear trend – providing approx. the same pixel noise value at all three levels). The figure confirms the problem of scanning at high resolution, during which big data scatter concerning measured *SD* values occurs.

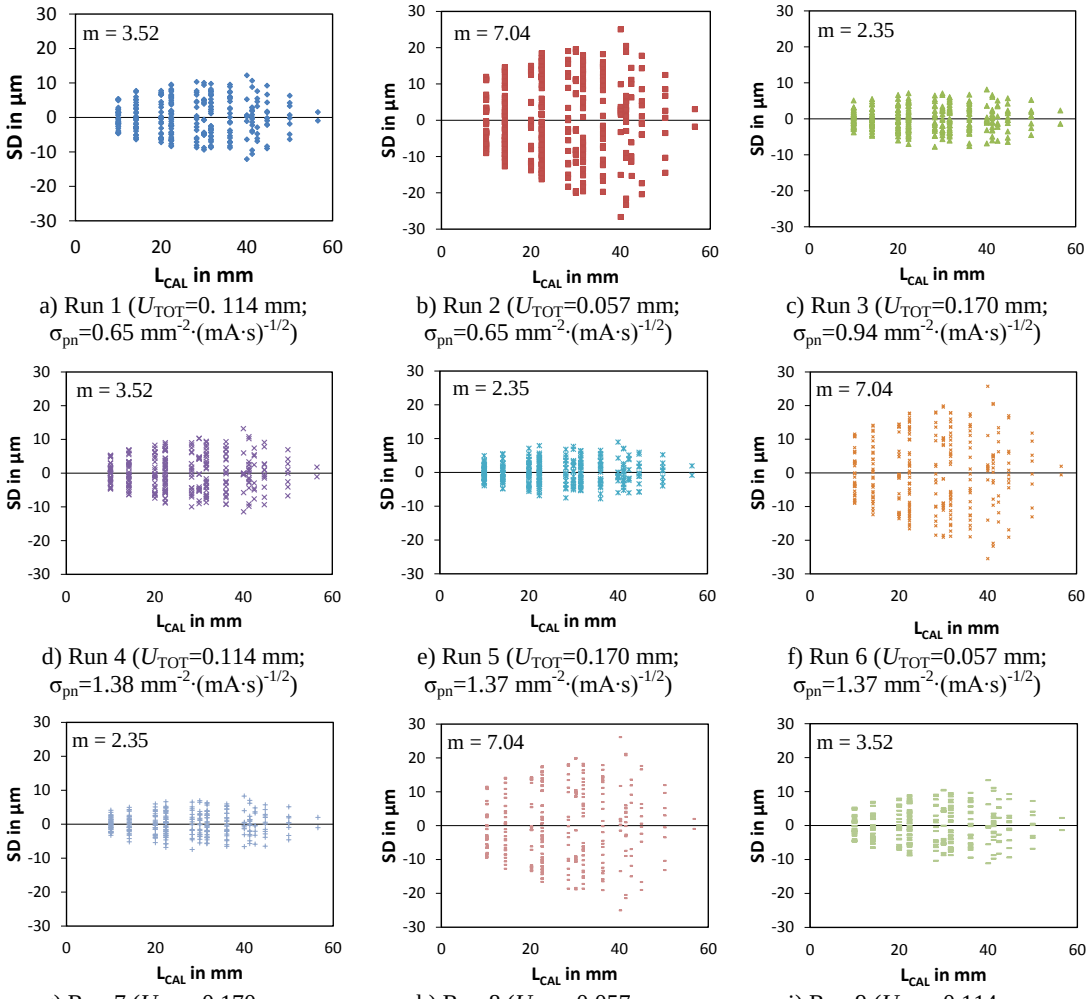

a) Run 1 (U_{TOT}=0. 114 mm; σ_{pn}=0.65 mm^{-2}·(mA·s)$^{-1/2}$)

b) Run 2 (U_{TOT}=0.057 mm; σ_{pn}=0.65 mm^{-2}·(mA·s)$^{-1/2}$)

c) Run 3 (U_{TOT}=0.170 mm; σ_{pn}=0.94 mm^{-2}·(mA·s)$^{-1/2}$)

d) Run 4 (U_{TOT}=0.114 mm; σ_{pn}=1.38 mm^{-2}·(mA·s)$^{-1/2}$)

e) Run 5 (U_{TOT}=0.170 mm; σ_{pn}=1.37 mm^{-2}·(mA·s)$^{-1/2}$)

f) Run 6 (U_{TOT}=0.057 mm; σ_{pn}=1.37 mm^{-2}·(mA·s)$^{-1/2}$)

g) Run 7 (U_{TOT}=0.170 mm; σ_{pn}=0.65 mm^{-2}·(mA·s)$^{-1/2}$)

h) Run 8 (U_{TOT}=0.057 mm; σ_{pn}=0.94 mm^{-2}·(mA·s)$^{-1/2}$)

i) Run 9 (U_{TOT}=0.114 mm; σ_{pn}=0.94 mm^{-2}·(mA·s)$^{-1/2}$)

Figure 4: Sphere distance errors calculated as a difference between CT and CMM measurements. L_{CAL} is the sphere-to-sphere calibrated length. Results are shown for all the nine runs of the experiment, as specified in Table 1. U_{TOT} and σ_{pn}, specified in the brackets, are the calculated spatial resolution and the calculated pixel noise, respectively. *m* is magnification. The original voxel data set is corrected for scale errors using linear regression.

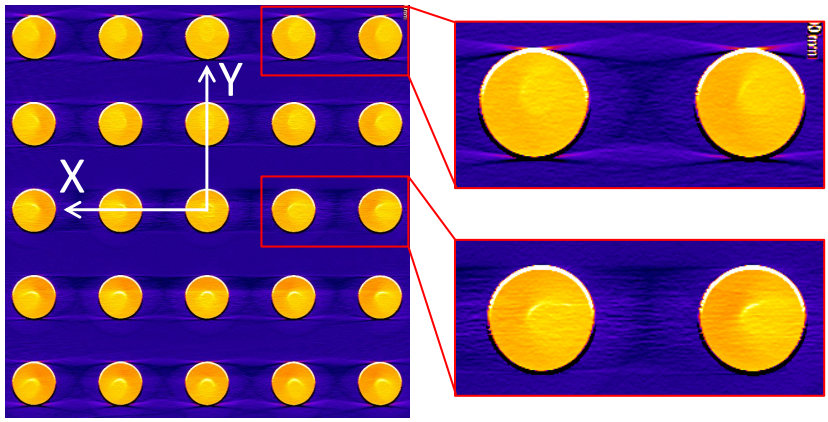

Figure 5: Slice of the reconstructed image for Run 2 of the experiment with high resolution (U_{TOT} = 0.057 mm; α=16.2°), taken in the XY plane of the CT scanner's coordinate system. Image artifacts can be recognized on the spheres positioned close to the upper and lower borders of the image, where Feldkamp effect is most pronounced. The orientation of this image is equivalent to position of the object in Figure 2 right.

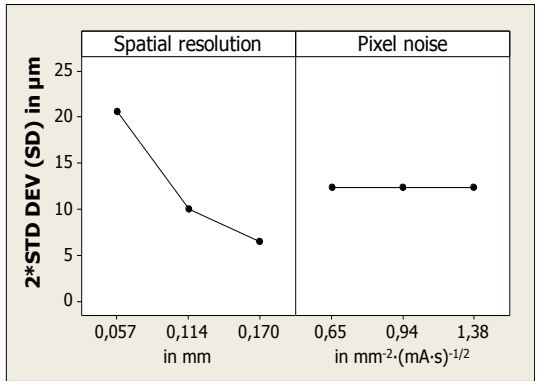

Figure 6: DOE results showing influence of the calculated spatial resolution (eq. 1) and the calculated pixel noise (eq. 4) on data scatter for calculation of the sphere distance error (*SD*), expressed as 2*standard deviation (STD DEV) of this parameter.

Since big errors were attributed to a position of the object close to the X-ray source (= high magnification) yielding big cone angle, further validation of the results should be done, in order to be able to make more general statements and conclusions about the proposed method. In particular, the CT ball plate should also be investigated at low magnification and, at the same time, at the upper or lower position at large opening angle. This could give an explanation to whether the errors come from the opening angle or any drift effect.

6 Experimental validation

From the results of the DOE analysis it appears that spatial resolution is a dominant factor having a great influence on dimensional measurements. In contrast, pixel noise seems not to have a visible influence for the selected scanning parameters and the selected measurand *SD*. Therefore, in the following, reconstruction images were analyzed for image quality.

It is known that in general, CT scans produced at higher spatial resolution lead to an increased noise [19]. This was also confirmed in our case – low SNR was measured on reconstructed images for CT scans at high resolution (see Figure 7). SNR was measured in the XZ plane of the CT scanner's coordinate system on a middle sphere, by selecting a region of interest (ROI) positioned in the center of the sphere (see Figure 8). The same ROI was applied to measure the SNR values for all the runs of the experiment. SNR is determined as a ratio between average gray values (signal) in the ROI, μ, and associated standard deviation of the gray values (noise), σ.

As three levels of pixel noise were theoretically specified according to eq. 4, three levels of SNR were expected to be measured. This was validated in the experiment and can be seen in Figure 7, where, clearly three levels of SNR are plotted at three associated levels of spatial resolution. The results are in a good agreement with the theory, i.e. the experimentally obtained values of SNR increase when pixel noise decreases. It can also be observed that the range of SNR values is bigger at lower spatial resolution and vice versa. The authors believe that the levels for pixel noise should have been selected in a wider range, where the influence of the pixel noise is bigger (see results of pixel noise in Figure 6). It should also be noted that each data point in the figure has an attributed uncertainty derived from the assessment of the SNR values, which might be influenced e.g. by the size and position of the ROI.

Since the first term in eq. 4 does not take into account spatial resolution, but a voxel size, this formula should be extended with this factor. It appears that the voxel size in the formula does not have big effect on pixel noise and thus the influence of spatial resolution can be underestimated.

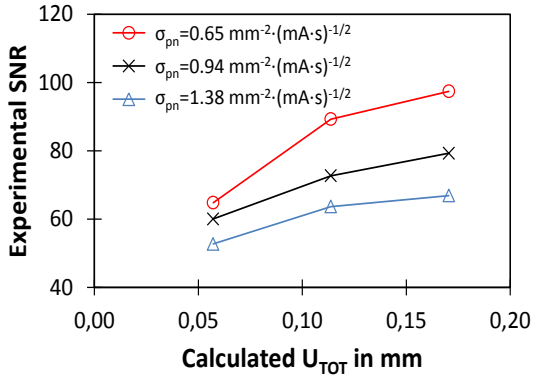

Figure 7: Signal-to-noise ratio (SNR) measured on reconstruction slices, showing low SNR for high resolution CT scans and vice versa.

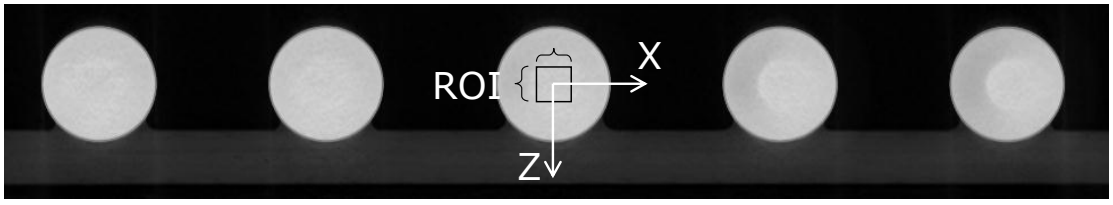

Figure 8: Selection of the ROI for measurements of the SNR. The slice was taken in the XZ plane of the CT scanner's coordinate system.

7 Conclusion

This paper describes a method allowing systematical analysis of measurement errors which occur in the volume of the CT system. The method is based on defining factors through combination of

scanning parameters. A CT ball plate, a reference standard featuring 25 ruby spheres glued on a carbon fibre plate, was used in this work to investigate the influence of image quality on dimensional CT measurements. Image quality was assessed in terms of spatial resolution and pixel noise. Both factors were determined theoretically. Measurement accuracy was determined by the analysis of sphere distance errors *SD*. In the following, several conclusions from this investigation are drawn:

- Results of the *SD* parameter have shown that by selecting proper combination of scanning parameters, minimization of these errors down to 10 µm, compared to the worst case being approx. 30 µm, can be achieved. Greater errors were found for CT scans at high resolution, i.e. for a position of the object close to the X-ray source where spheres are imaged at large opening angle. At this position, image artifacts, probably caused by the Feldkamp effect, as well as to a minor extent focus spot drift or rotary axis drift, were pronounced.
- The DOE analysis has shown the spatial resolution being dominant factor and thus, having a big influence on dimensional measurements. In contrast, the pixel noise appeared not to be significant. However, this was only investigated for the selected parameter *SD* and the limited number of runs of DOE under study.
- The theoretical formulation of pixel noise was experimentally validated by analyzing images obtained from a reconstruction volume. As three levels of pixel noise were theoretically defined, three levels (values) of SNR were expected. These were found in a well-specified ROI and thus, it can be concluded that the experiment is in a good agreement with theory. Moreover, with decreased pixel noise, increase of SNR values was observed. The three levels of SNR were more distinctive for CT scans at low resolution. Most likely, the levels for pixel noise should have been selected in a wider range, where the influence of the pixel noise is more significant.
- The presented approach seems to be a promising method for prediction and optimization of scanning parameters.

8 Outlook

- The authors believe that the proposed experimental design can be adapted to real workpieces and it is therefore an intention to investigate into what extent this design can be applied.
- Further validation of the proposed method should be done, in order to be able to make more general conclusions. In particular, the CT ball plate should also be investigated at low magnification and, at the same time, at the upper or lower position at large opening angle.
- Further analysis should be carried out to investigate the effect of the two factors (spatial resolution and pixel noise) on other parameters than *SD*, e.g. probing errors *PF* and *PS*, or threshold effects by the assessment of bidirectional length measuring errors *E*.
- Further, experimental validation of spatial resolution is necessary, since this was not done in the present work. Spatial resolution can be experimentally determined using e.g. wires (cylinders), spheres, edges [8, 10, 13].

Acknowledgement

The authors would like to thank Physikalisch-Technische Bundesanstalt (Braunschweig, Germany) for kindly providing the CT scanner and assisting with the setup and CT measurements.

References

[1] J.P. Kruth, M. Bartscher, S. Carmignato, R. Schmitt, L. De Chiffre, A. Weckenmann, Computed Tomography for Dimensional Metrology, Annals of CIRP, Vol 60/1, 821–842, 2011.
[2] M. Bartscher, U. Hilpert, J. Goebbels, G. Weidemann, Enhancement and Proof of Accuracy of Industrial Computed Tomography (CT) Measurements, Annals of CIRP, Vol 56/1, 495-498, 2007.
[3] R. Schmitt, Ch. Niggemann, Uncertainty in measurement for x-ray-computed tomography using calibrated workpieces, Measurement Science and Technology, Vol 21, 054008, 2010.
[4] A. Weckenmann, P. Krämer, Predetermination of measurement uncertainty in the application of computed tomography, 11th CIRP International Conference on Computer Aided Tolerancing, 2009.
[5] S. Carmignato, Traceability of dimensional measurements in computed tomography, In: Proceedings of 8th A.I.Te.M. Conference, 2007.
[6] U. Hilpert, M. Bartscher, M. Neugebauer, J. Goebbels, G. Weidemann, C. Bellon, Simulation-aided computed tomography (CT) for dimensional measurements, International Symposium on Digital industrial Radiology and Computed Tomography, 2007.
[7] P. Müller, J. Hiller, A. Cantatore, L. De Chiffre, Investigation of measuring strategies in computed tomography, In: Proceedings of the International conference on Advanced Manufacturing Engineering (NEWTECH 2011), 31-42, 2011.
[8] W.A. Kalender, Computed Tomography: Fundamentals, System Technology, Image Quality, Applications, 260 pages, 2006.
[9] J. Hiller, T.O.J. Fuchs, L.M. Reindl, Influence of the quality of X-ray computed tomography image on coordinate measurements: Principles, measurements and simulations, Technisches Messen, Vol 78/7-8, 334-347, 2011.
[10] J. Hiller, M. Maisl, L. M. Reindl, Physical characterization and performance evaluation of an x-ray micro-computed tomography system for dimensional metrology applications, Measurement Science and Technology, 2012, in press.
[11] VDI/VDE 2630/Part 1.1 Computed tomography in dimensional measurement, Basics and definitions, July 2009.
[12] M.J. Flynn, S.M. Hames, D.A. Reimann, S.J. Wilderman, Microfocus X-ray sources for 3D microtomography, Nuclear Instruments and Methods in Physics Research A, Vol 353, 312-315, 1994.
[13] X. Yang, Y. Meng, Q. Luo, H. Gong, High resolution in vivo micro-CT with flat panel detector based on amorphous silicon, Journal of X-Ray Science and Technology, Vol 18/4, 381-392, 2010.
[14] ISO 15708-1:2002. Non-destructive testing -- Radiation methods -- Computed tomography -- Part 1: Principles. ISBN-10: 3895782165.
[15] P. Müller, J. Hiller, A. Cantatore, G. Tosello, L. De Chiffre, New reference object for metrological performance testing of industrial CT systems, In: Proceedings of the 12th International Conference of the European Society for Precision Engineering & Nano Technology (euspen), 72-75, 2012.
[16] VDI/VDE 2630/Part 1.3 Computed tomography in dimensional measurement, Guideline for the application of DIN EN ISO 10360 for coordinate measuring machines with CT sensors, August 2009.
[17] J. Hiller, S. Kasperl, U. Hilpert, M. Bartscher, Coordinate measuring with industrial X-ray computed tomography, Technisches Messen, Vol 74/11, 553-564, 2007.
[18] D. Weiss, A. Deffner, C. Kuhn, Einfluss der Quellbewegung auf Reproduzierbarkeit und Antastabweichung im Röntgen-Computertomographen, Proceedings Fachtagung Industrielle Computertomographie (CTC), 2010.
[19] J. Hsieh, Computed Tomography: Principles, Design, Artifacts, and Recent Advances, Second Edition (SPIE Press Book), Vol PM188, 2003.